

# MARS: A NEUROSYMBOLIC APPROACH FOR INTERPRETABLE DRUG DISCOVERY

**Lauren Nicole DeLong**

AI & its Applications Institute  
School of Informatics  
University of Edinburgh  
L.N.DELONG@sms.ed.ac.uk

**Yojana Gadiya**

Enveda Biosciences  
Boulder, CO, USA  
yojana.gadiya@envedabio.com

**Paola Galdi**

AI & its Applications Institute  
School of Informatics  
University of Edinburgh  
paola.galdi@ed.ac.uk

**Jacques D. Fleuriot**

AI & its Applications Institute  
School of Informatics  
University of Edinburgh  
jacques.fleuriot@ed.ac.uk

**Daniel Domingo-Fernández**

Enveda Biosciences  
Boulder, CO, USA  
daniel.domingo-fernandez@envedabio.com

## ABSTRACT

Neurosymbolic (NeSy) artificial intelligence describes the combination of logic or rule-based techniques with neural networks. Compared to neural approaches, NeSy methods often possess enhanced interpretability, which is particularly promising for biomedical applications like drug discovery. However, since interpretability is broadly defined, there are no clear guidelines for assessing the biological plausibility of model interpretations. To assess interpretability in the context of drug discovery, we devise a novel prediction task, called drug mechanism-of-action (MoA) deconvolution, with an associated, tailored knowledge graph (KG), *MoA-net*. We then develop the *MoA Retrieval System (MARS)*, a NeSy approach for drug discovery which leverages logical rules with *learned* rule weights. Using this interpretable feature alongside domain knowledge, we find that MARS and other NeSy approaches on KGs are susceptible to reasoning shortcuts, in which the prediction of true labels is driven by “degree-bias” rather than the domain-based rules. Subsequently, we demonstrate ways to identify and mitigate this. Thereafter, MARS achieves performance on par with current state-of-the-art models while producing model interpretations aligned with known MoAs.

## 1 INTRODUCTION

Drug discovery (DD), the search for novel drugs or chemical compounds to treat ailments, often involves the screening of thousands of small compounds (Lin et al., 2020). Many computational approaches have been developed to accelerate and streamline this screening process (Gottlieb et al., 2011; Gan et al., 2023). Specifically, hundreds of such approaches operate upon knowledge graphs (KGs), in which nodes representing drugs, proteins, or medical conditions are connected by edges, representing the relationships between them (Chen et al., 2020). Typically, DD is formulated on a KG as a link prediction task between drugs and the corresponding medical conditions (indications) to be treated (Schultz et al., 2021; Rivas-Barragan et al., 2022).

Moreover, it is important to understand each drug’s mechanism-of-action (MoA), the molecular processes by which it achieves its medicinal effect. For instance, one drug, cortisone acetate, up-regulates the activity of the glucocorticoid (GC) receptor protein, which, in turn, downregulates the cyclooxygenase (COX) protein. Since the COX protein is involved in creating inflammation, its

inhibition reduces inflammation (Gonzalez-Cavazos et al., 2023). Thus, MoAs typically involve chains of physical, molecular interactions induced by a drug. Uncovering these interactions informs researchers as to how each drug works and de-risks potential side effects (Palve et al., 2021; Green et al., 2023).

However, revealing MoAs alongside computational DD, a task we call *MoA deconvolution*, requires model interpretability: transparency into the processes or patterns which led to certain predictions (Molnar, 2022). Unfortunately, most state-of-the-art techniques on KGs rely on “black-box” models (Wu et al., 2020). Recently, neurosymbolic (NeSy) approaches, which combine logical rules with neural networks (DeLong et al., 2024) have been positioned as a promising avenue for MoA deconvolution. Specifically, NeSy methods tend to possess enhanced interpretability and better integrate structured domain knowledge, of which there is plenty in biomedicine (Acharya et al., 2023; Rigden & Fernández, 2023). However, since interpretability is broadly defined, there are no clear guidelines for assessing the plausibility of model interpretations, especially for this novel task (Molnar, 2022).

Thus, we propose MoA deconvolution as a prediction task for evaluating *interpretable* methods on KGs. We generate a tailored KG for benchmarking this task, *MoA-net*. To perform MoA deconvolution, we introduce a NeSy DD approach called the MoA Retrieval System (MARS). To create MARS, we draw inspiration from previous NeSy methods (Liu et al., 2020; Drancé et al., 2021). However, unlike its predecessors, MARS leverages logical rules with *learned* rule weights. Following training, rule weights reflect relative usefulness to MARS’ reasoning processes.

Alongside biomedical domain knowledge, MARS’ enhanced interpretability reveals a reasoning shortcut in which predictions are based on unintended semantics (Marconato et al., 2024b). Essentially, predictions upon *MoA-net* are driven by “degree-bias”, an artifact of node degree variance (Zietz et al., 2024), rather than the rules representing domain knowledge. Therefore, to address this second challenge, we consider the desiderata from Marconato et al. (2024a) for making NeSy systems *shortcut-aware*: (1) *calibration*, high accuracy on concepts unaffected by reasoning shortcuts, (2) *performance*, high accuracy despite reasoning shortcuts being present, and (3) *cost effectiveness* achieved through simple mitigation strategies. Using these desiderata as guidelines, we make MARS shortcut-aware for more insightful predictions involving DD and MoA deconvolution. Ultimately, our study underscores the importance of evaluating the capabilities of NeSy models within applied domains: by evaluating model interpretations against specific domain knowledge, we can more easily identify and mitigate shortcuts.

**Contributions.** In summary, our work:

1. devises a novel prediction task, MoA deconvolution, to assess the interpretability of NeSy and other KG-based approaches;
2. provides a novel biomedical KG, *MoA-net*, on which MoA deconvolution can be benchmarked;
3. presents the MoA retrieval system, MARS, a NeSy approach with enhanced interpretability through dynamic rule-weight updates;
4. through MARS’ enhanced interpretability, identifies a key reasoning shortcut affecting some NeSy models;
5. demonstrates ways to test and mitigate this reasoning shortcut, making MARS shortcut-aware and better aligned with domain knowledge.

## 2 RELATED WORK AND BACKGROUND

**Drug Discovery and MoA Deconvolution.** Amongst previous open-source approaches for DD, many focus on drug repositioning (DR), as opposed to finding novel compounds (Rivas-Barragan et al., 2022; Urbina et al., 2021; Zheng et al., 2019). DR aims to discover new uses for drugs that have already been approved for distribution (Urbina et al., 2021). This prediction task allows researchers to leverage more available knowledge on approved drugs, including recorded clinical outcomes and side effects (Ratajczak et al., 2022; Liu et al., 2020). However, such relations are revealed during or after clinical trials, and are therefore rare or unknown for *novel* compounds. Furthermore, with such relations present, DR models oftentimes rely on *associative* patterns (e.g., drugs causing the

same side effects also likely share indications) rather than *mechanistic* ones (e.g., involving physical, molecular interactions). Therefore, such models offer limited insight into drug MoAs.

**NeSy AI for KGs.** Several NeSy approaches for KGs involve logical rules in which the rule bodies reflect path-like patterns in the KG (e.g.,  $\text{treats}(A, D) \leftarrow \text{targets}(A, B) \wedge \text{regulates}(B, C) \wedge \text{attenuates}(C, D)$ ) (Liu et al., 2020; Dash & Goncalves, 2021; Sen et al., 2021). This is ideal for investigating MoAs, which typically occur as consecutive chains of molecular interactions (Crino, 2016). Some of these approaches utilize deep reinforcement learning (RL), in which a neural network contributes toward the optimization of a reward function (Acharya et al., 2023). In these specific cases, the reward function is partially determined by whether an agent’s trajectory through the KG corresponds to a rule body, thereby satisfying a rule. Therefore, the agent is *guided* by the path-like rules, and predictions are expected to align, to some extent, with such rules. In this study, however, we also identify a major risk: the agent will ignore rules if it can exploit *other* semantics for reward optimization. This results in *reasoning shortcuts*.

**Reasoning Shortcuts.** Several NeSy approaches are designed to abide by rules and domain knowledge (Drancé et al., 2021; Dash & Goncalves, 2021), which might portray such approaches as more trustworthy than neural, black box ones (Gaur & Sheth, 2024). Recent studies, however, have found that NeSy approaches may suffer from reasoning shortcuts, in which a model predicts the correct outcome via unintended semantics (Marconato et al., 2024b; Li et al., 2024b). While reasoning shortcuts are not exclusive to NeSy methods (Jiang & Bansal, 2019; Li et al., 2024a), they may be more easily overlooked when such approaches are portrayed as trustworthy.

### 3 MARS: A NESY APPROACH FOR MOA DECONVOLUTION

Here, we build the MoA Retrieval System (MARS)<sup>1</sup> to perform MoA deconvolution. MARS improves upon a method called Policy-guided walks with logical rules (PoLo) (Liu et al., 2020) by introducing dynamic, *learned* rule weights. This differs from previous approaches, where weights are static and pre-computed (e.g., mined or literature-derived) (Liu et al., 2020; Drancé et al., 2021). As discussed further, these learned weights make MARS shortcut-aware.

MARS takes two major inputs. The *first* is a KG. A KG uses nodes to represent entities and edges between them to represent relationships. A KG *triple* comprises two nodes connected by an edge of some specific type, or *relation*. For example, *interacts*(*Protein*, *Protein*) states that two *Protein* nodes are connected via the *interacts* relation. *Node degree* describes the number of edges connected to a node.

Specifically, the input KG must contain triples involving some relation of interest. To understand each MoA as the biological response to drug administration, we aim to investigate relations between drugs and biological processes (BPs), such as *signal transduction* or *inflammation* (Consortium, 2019) (*i.e.*, *induces*(*Drug*, *BP*)). As per our knowledge, this is a novel application in the KG field. Further details on our KG are introduced within section 3.4. The *second* input includes metapaths of the KG with corresponding weights.

#### 3.1 METAPATH-BASED RULES

Metapaths are abstract representations of instantiated paths in a graph (Sun et al., 2011; Himmelstein et al., 2017; Noori et al., 2023). For example, given the following path,  $P$ , in our KG:

$$\text{Cortisone acetate} \xrightarrow{\text{upregulates}} \text{GC receptor} \xrightarrow{\text{interacts}} \text{COX protein} \xrightarrow{\text{participates}} \text{Inflammation}$$

the corresponding metapath,  $\tilde{P}$ , would be:

$$\text{Drug} \xrightarrow{\text{upregulates}} \text{Protein} \xrightarrow{\text{interacts}} \text{Protein} \xrightarrow{\text{participates}} \text{Biological Process}$$

Within this study, metapaths can be understood as a sequence of relations within the KG structure, making them inherently interpretable. In MARS, metapaths are used as the bodies of logical rules, in

<sup>1</sup><https://github.com/laurendelong21/MARS>

which the rule head, the left side of the implication arrow ( $\Leftarrow$ ), constitutes a single, binary predicate representing the relation of interest between the first and last node types, *e.g.*:

$$\text{induces}(Drug, BP) \Leftarrow \text{upregulates}(Drug, Protein_A) \wedge \\ \text{interacts}(Protein_A, Protein_B) \wedge \text{participates}(Protein_B, BP)$$

For each metapath-based rule,  $M_i$ , in the set of feasible rules,  $\mathcal{M} = \{M_1, M_2, \dots, M_m\}$ , we denote the rule weight by  $w(M_i) \in \mathbb{R}$ , where  $0 \leq w(M_i) \leq 1$ . Such a weight indicates the relative usefulness of the metapath-based rule to the prediction task. In Section 3.3, we discuss how we initialize and compute these weights.

### 3.2 OVERVIEW OF MARS.

Using a deep RL process, MARS trains an agent to take walks of length  $L$  through the KG to connect pairs of nodes having the pre-defined relation of interest (*e.g.*, `induces`); such edges are masked from the agent during training. Each walk generates a path,  $P$ , which can be understood as a series of  $L$  transitions:  $P := (e_c \xrightarrow{r_1} e_2 \xrightarrow{r_2} \dots \xrightarrow{r_L} e_{L+1})$ . The agent may also remain at its current node. Ultimately, the goal of the agent is episodic: to find paths in which the starting node,  $e_c$ , and the terminal node,  $e_{L+1}$ , make up one of the true input pairs. By training the agent to do so, it can identify node pairs with some desired relationship, thus generalizing beyond the training set to predict novel pairs. Through a process akin to a Markov Decision Process (Bellman, 1957), the agent makes decisions about its next move based on information about its current position and the next possible actions. Additionally, however, the history of the agent’s previous actions are encoded with an LSTM (Hochreiter & Schmidhuber, 1997; Sherstinsky, 2020), whose parameters are trained to optimize the reward function,  $R(S_{L+1})$  (Eq. 1), which is evaluated each time the agent completes  $L$  transitions from some starting node, reaching a state  $S_{L+1}$ :

$$R(S_{L+1}) = \mathbb{1}_{\{e_{L+1}=e_d\}} + \mathbb{1}_{\{e_{L+1}=e_d\}} \lambda \sum_{i=1}^m w(M_i) \mathbb{1}_{\{\tilde{P}=M_i\}} \quad (1)$$

$$\mathbb{1}_{\{A\}} = \begin{cases} 1 & \text{if } A = \text{true} \\ 0 & \text{if } A = \text{false} \end{cases} \quad (2)$$

This reward function, adapted from Liu et al. (2020), quantifies how successful  $P$  is according to two summands, where the hyperparameter  $\lambda$  influences the balance between them. The first summand indicates whether the terminal node in the path,  $e_{L+1}$ , is one of the desired target (BP) nodes ( $e_d$ ) that forms a true pair with the starting (drug) node,  $e_c$ . The second summand, contingent upon the first, indicates whether the corresponding metapath,  $\tilde{P}$ , matches any metapath-based rule,  $M_i$ . Therefore, the agent is not only encouraged to find connections between true pairs of nodes, but it is also guided toward paths which resemble known MoAs. Implementation details and hyperparameter selection are described in Appendices A.2 and A.4, respectively.

Of note, the second summand is proportional to some metapath-based rule weight, and MARS updates these weights during training. We accomplish this through a novel algorithm we call *two-hop joint probability*, or  $P_{2H}$ .

### 3.3 WEIGHT UPDATES VIA 2-HOP JOINT PROBABILITY

After MARS is executed, its learned rule weights reflect each rule’s relative usefulness in the prediction task. Additionally, during training, weight updates drive the agent toward more informative paths and bypass the assumptions that pre-assigned rule weights are correct and informative. This eliminates the need for pre-computed or literature-derived rule weights; therefore, we initialize all weights uniformly as 0.5, a *medium* level of importance.

The naive way to implement weight updates (MARS<sub>naive</sub>) is to increase weights according to the frequency at which each metapath-based rule is satisfied. However, this would not account for partial metapath matches. As an alternative, we propose updates via two-hop joint probability ( $P_{2H}$ ). This metric approximates the usefulness of metapath-based rules based on the observed frequencies of the two-hop fragments that they comprise. Since the metapaths constituting rule bodies typically

contain three or four consecutive relations, each two-hop fragment is extracted as in the following example:

$$M_{example} := \text{induces}(A, E) \Leftarrow \text{upregulates}(A, B) \wedge \text{interacts}(B, C) \wedge \text{interacts}(C, D) \wedge \text{participates}(D, E)$$

where two-hop fragments are pairs of binary predicates which share a variable:

- *Fragment1* :  $\text{upregulates}(X, Y) \wedge \text{interacts}(Y, Z)$
- *Fragment2* :  $\text{interacts}(X, Y) \wedge \text{interacts}(Y, Z)$
- *Fragment3* :  $\text{interacts}(X, Y) \wedge \text{participates}(Y, Z)$

Here, the probability of each metapath-based rule is computed as the joint probability of its fragments. For example, the  $P_{2H}$  metric for the above metapath-based rule would be computed as  $P_{2H}(M_{example}) = p(\text{Fragment1}) \times p(\text{Fragment2}) \times p(\text{Fragment3})$ . The probability of each fragment is determined by the ratio of its observed and expected frequencies (see Appendix A.3). We note that, while the fragments do not necessarily represent independent events, the way in which  $P_{2H}$  is computed imposes this assumption. To compute the joint probability for dependent events, we require the conditional probabilities of the dependent events (Russell & Norvig, 2010). This can, in theory, be computed, but it becomes more complex with metapath length. For simplicity's sake, we assume independence, and the  $P_{2H}$  metric serves as an *approximation* for the empirical probabilities of metapath-based rules. Further formalization and pseudocode are in Appendix A.3. Ultimately, MARS with  $P_{2H}$  updates ( $\text{MARS}_{P_{2H}}$ ) uses *all* information from successful trajectories.

### 3.4 DATASETS: *MoA*-net AND ITS VARIANTS

We design our KG, *MoA*-net<sup>2</sup>, specifically for MoA prediction. *MoA*-net consists of drugs, proteins, and BPs (Fig. 1-A). We assemble it using the causal relations between drugs and proteins from Custom KG (Rivas-Barragan et al., 2020) and OpenBioLink KG (Breit et al., 2020). The BP nodes come from molecular function annotations in UniProt (Consortium, 2015).

To predict drug-BP triples, which are unique to *MoA*-net, we make use of publicly available functional and biochemical assays in ChEMBL (v33), an open access database of bioactive compounds (Gaulton et al., 2012). Of the 1,622 drug-BP triples obtained, 48 also had *known* MoAs in *DrugMechDB* (Gonzalez-Cavazos et al., 2023), a manually-curated compendium of MoAs. Between the three node types, we define five unique edge types, or relations, shown in Fig. 1-B. We also include all inverse relations, running in the opposite direction of causality.

Using the *hetnetpy* package (Himmelstein et al., 2021), we extract all metapaths (see Section 3.1) from *MoA*-net which we considered to be valid MoAs: those comprising directed, mechanistic paths between drug and BP nodes (see Appendix A.1). Although other metapaths are possible, we exclude them from our set of metapath-based *rules*. Based on MoAs found in *DrugMechDB*, we limit metapaths to a maximum length of four relations (or *hops*).

Finally, we create variants of *MoA*-net. To investigate reasoning shortcuts, we use the Zietz et al. (2024) implementation of XSwap (Hanhijärvi et al., 2009), which swaps edges in a KG without affecting the distribution of node degrees. We call the resultant KG *MoA*-net-*permuted*. Additionally, we implement an automatic trimming step, which reduces edges of each class to below a user-specified threshold by iteratively removing those between the highest-degree nodes. By setting the threshold to 10,000 (thereby reducing protein-protein interactions to  $\sim 50\%$  of edges), our approach can work on a subgraph of the *MoA*-net, which we refer to as *MoA*-net-10k.

### 3.5 EVALUATION

We split the drug-BP triples within *MoA*-net into training (60%), validation (20%), and test (20%) sets. We evaluate the models using Hits@ $k$ , where  $k \in \{1, 3, 10\}$  and mean reciprocal rank (MRR), optimizing for the latter. Hits@ $k$  reports the proportion of times the correct results are in the top  $k$  ranked entries, while MRR reports how highly ranked the first correct item is amongst ranked results (Chen et al., 2020). In addition to these *standard* metrics, we report the *pruned* metrics: these are

<sup>2</sup><https://github.com/laurendelong21/MoA-Net>

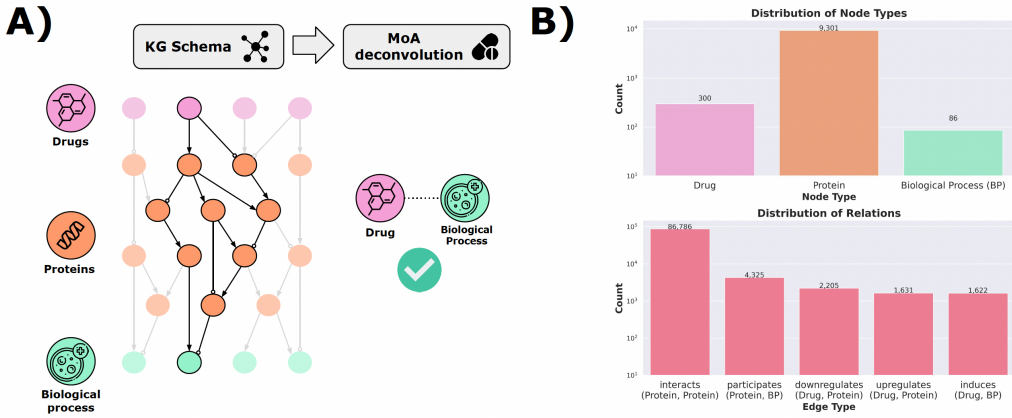


Figure 1: A) *MoA*-net schema. B) Distribution of node and relationship types of *MoA*-net. Note that the *y*-axis has a logarithmic scale.

computed on a subset of the predictions that utilized one of the pre-defined metapath-based rules (see Appendix A.1), excluding all predictions which did not satisfy a rule. Notably, pruned metrics help us assess the *calibration* desideratum, as introduced in Section 1, since rule-based predictions follow the expected model semantics.

We conduct an extensive benchmark of our method against nine different baseline KG embedding (KGE) models, two state-of-the-art NeSy methods, and one network measure. Based on previous biomedical KG benchmarks (Rivas-Barragan et al., 2022), the KGE models include RESCAL (Nickel et al., 2011), TransE (Bordes et al., 2013), DistMult (Yang et al., 2014), ER-MLP (Dong et al., 2014), ComplEx (Trouillon et al., 2016), HOLE (Nickel et al., 2016), ConvE (Dettmers et al., 2018), RotatE (Sun et al., 2019) and MuRE (Balazevic et al., 2019). We also compare against PoLo (Liu et al., 2020) and its predecessor MINERVA (Das et al., 2018), which optimizes only the first summand of the reward function (*i.e.*,  $\lambda = 0$  in Eq. 1). Additionally, we test prioritization of drug-BP triples based on degree-weighted path count (DWPC) using 0.4 as damping exponent (Himmelstein & Baranzini, 2015). We train and evaluate these models on the same data splits as MARS on *MoA*-net-10k.

Finally,  $MARS_{P_{2H}}$  has two key interpretable features: firstly, all successful trajectories are recorded, serving as potential MoA predictions. This allows us to compare the predicted MoAs of 48 drug-BP pairs against their known MoAs (see Section 3.4). Secondly, learned rule weights serve as a proxy for the importance of each metapath-based rule. This helps determine whether agent trajectories are biased toward certain types of paths. Alongside the pruned metrics, these features help evaluate MARS’ alignment with domain knowledge.

## 4 RESULTS

### 4.1 ASSOCIATIVE PATTERNS IMPROVE ACCURACY BUT OFFER LIMITED PRACTICAL USE

In an initial set of experiments on *MoA*-net, we observed that pruned metrics were consistently lower than standard ones (Fig. 2-A), indicating that the metapath-based rules were not being utilized in most predictions. This can happen because rule-based rewards are contingent upon a true pair being found (Eq. 1). Additionally, amongst recorded trajectories, most did *not* follow our metapath-based rules; instead, most trajectories used the following metapath, involving inverse edges:

$$\text{induces}(Drug_1, BP_2) \Leftarrow \text{induces}(Drug_1, BP_1) \wedge \text{induces}(Drug_2, BP_1) \wedge \text{induces}(Drug_2, BP_2)$$

This associative pattern indicates that two drugs inducing a common BP also likely induce another BP. This type of pattern is also present in a previous NeSy RL study, Liu et al. (2020), in which the most used metapath was the following:

$$\text{treats}(Drug_1, Disease) \Leftarrow \text{causes}(Drug_1, Side\ Effect) \wedge \\ \text{causes}(Drug_2, Side\ Effect) \wedge \text{treats}(Drug_2, Disease)$$

However, when we reproduced the results from Liu et al. (2020), we achieved the same reported metrics even in the absence of the above, associative rule (See Appendix A.5). This suggests that, although the associative rule may serve as a *plausible* model explanation, it does not necessarily guide model training.

Previously, associative patterns have been regarded as informative in other KG prediction tasks such as DR and target prediction (Fernández-Torras et al., 2022; Ratajczak et al., 2022; Himmelstein et al., 2017; Renaux et al., 2023; Li et al., 2023; Muslu et al., 2020). However, associative patterns do *not* constitute biologically valid MoAs. As stated in Section 1, MoAs, like those in *DrugMechDB*, involve physical, molecular interactions. Therefore, an MoA path would not traverse an additional drug node. In other words, while such associations may be a valid proxy for other biomedical tasks, MoA deconvolution for novel compounds is inherently limited to information around its protein targets and related BPs.

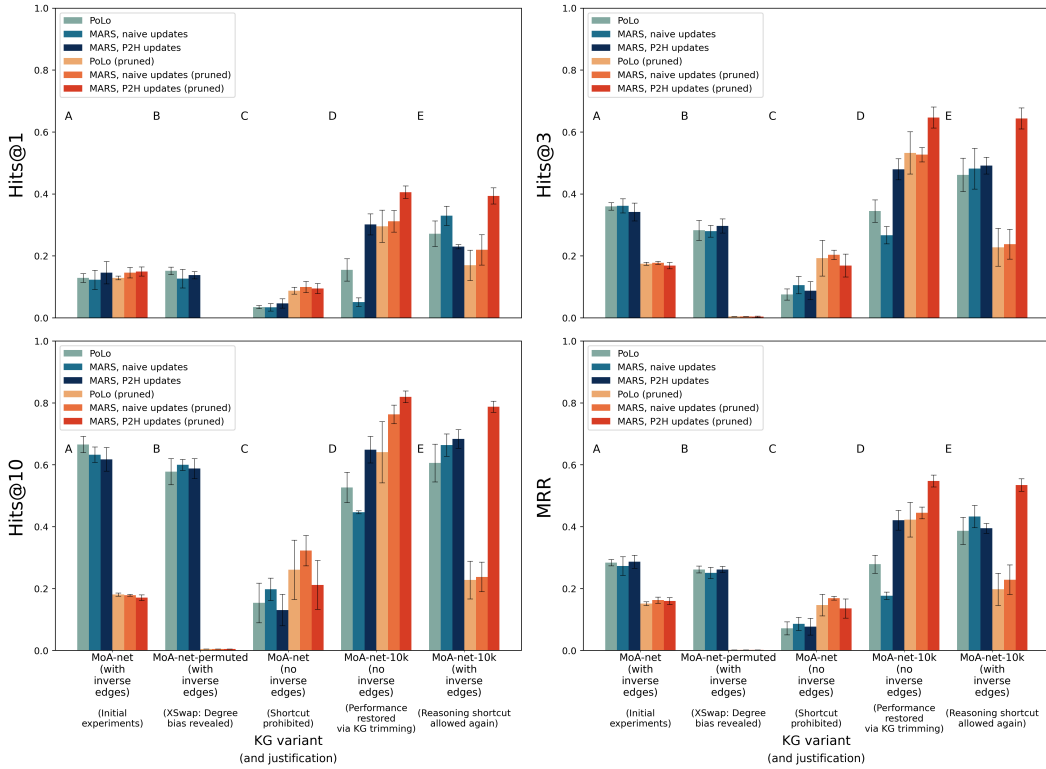


Figure 2: Performance metrics for  $MARS_{P2H}$  compared to PoLo and  $MARS_{naive}$  upon several variants of *MoA-net*. Each bar is the average and standard deviation across five independent training and testing iterations. From left to right: Little change between initial metrics upon *MoA-net* (A) in comparison to the standard *MoA-net-permuted* metrics (B) provides evidence that predictions are influenced by degree bias, resulting in a reasoning shortcut. Thereafter, inverse edges were removed to prohibit the reasoning shortcut, hindering performance (C). Performance was restored upon *MoA-net-10k* with the KG trimming step (D), with  $MARS_{P2H}$  showing the best standard and pruned metrics. Finally,  $MARS_{P2H}$  maintains high pruned metrics even when inverse edges (and reasoning shortcuts) are re-introduced (E).

#### 4.2 $P_{2H}$ UPDATES REVEAL REASONING SHORTCUTS VIA DEGREE BIAS

In addition to analyzing the agent trajectories, we used  $P_{2H}$  to assess how informative each of the metapath-based rules is in making predictions. In particular,  $MARS_{P2H}$  weights showed that paths involving consecutive protein-protein interactions (PPIs) (*i.e.*,  $\text{interacts}(Protein, Protein)$ ),

were consistently less important (Fig. 3). This indicated that the agent avoided exploring consecutive PPIs.

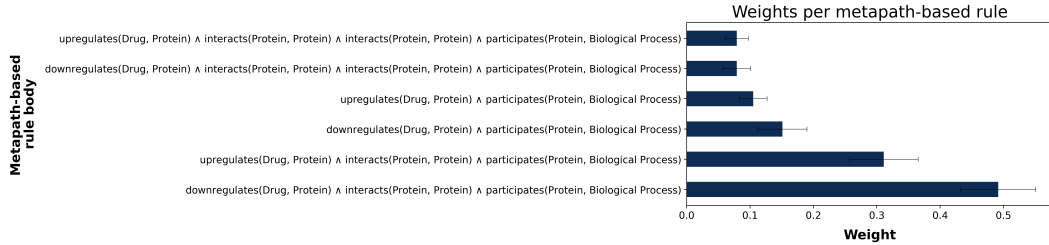


Figure 3: Metapath-based rule weights from  $MARS_{P_{2H}}$  on  $MoA\text{-}net$  (Fig. 2-A). Each bar is the average and standard error across five independent training and testing iterations. Paths involving consecutive PPIs ( $\text{interacts}(Protein, Protein)$ ), the most common relation type, have consistently lower weights.

Previous research on KGs has shown that node degree distribution, the number of adjacent edges for each KG node, can significantly bias predictions (Tang et al., 2020; Ju et al., 2024). Specifically, *inspection bias*, a type of degree bias, occurs when the KG is not uniformly inspected or sampled (Zietz et al., 2024). Since PPIs are the most common relation type in  $MoA\text{-}net$  (90% of edges) (Fig. 1-B), protein nodes have a higher degree distribution than other node types. We hypothesized, therefore, that the agent circumvents denser parts of the KG, creating an inspection bias. Although rule-based predictions merit a larger reward, the MARS agent exploits associative patterns for a more reliable reward. To confirm the existence of degree bias, we tested our approach upon  $MoA\text{-}net\text{-permuted}$ . As explained in Section 3.4,  $MoA\text{-}net\text{-permuted}$  is a variant of  $MoA\text{-}net$  in which edges are swapped while preserving node degree distribution. This tests the extent to which node degree drives predictions. Indeed, the lack of change amongst standard performance metrics suggested that node degree was largely responsible for predictions (Fig. 2-B). Put simply, the agent gets lost when exploring the PPIs, so it avoids them.

#### 4.3 IDENTIFYING AND MITIGATING DEGREE BIAS IMPROVES PERFORMANCE

To temporarily prohibit the models from using associative patterns as in Section 4.1, we removed inverse edges from  $MoA\text{-}net$  and corresponding metapath-based rules. Consequently, the performance metrics were poor, (e.g., MRR consistently  $< 0.1$  (Fig. 2-C)). This confirmed that the models relied on associative patterns for predictions.

Next, we wanted to confirm that the agent was getting lost within the PPIs. As explained in Section 3.4,  $MoA\text{-}net\text{-}10k$  is a variant of  $MoA\text{-}net$  with fewer PPIs. We tested  $MARS_{P_{2H}}$ ,  $MARS_{\text{naive}}$ , and PoLo with the same parameters upon on  $MoA\text{-}net\text{-}10k$  (Fig. 2-D). As before, we excluded inverse edges. Since we set trajectory length  $L = 4$ , our approach automatically removed drug-BP triples from the validation/test sets that were no longer connected via directed paths of length  $\leq 4$ , resulting in 100 and 90 triples, respectively. Metrics were markedly improved for PoLo,  $MARS_{\text{naive}}$ , and *particularly* for  $MARS_{P_{2H}}$ , in comparison to the full  $MoA\text{-}net$  without inverse edges (Fig. 2-C). To ensure this improvement was not simply the result of a reduced test set, we also tested the approaches upon  $MoA\text{-}net$  with 100 sampled test triples, which showed no change (see Appendix A.6).

While removing inverse edges improved metrics, a shortcut-aware system should achieve high *performance* even with the shortcut present (Marconato et al., 2024a). We addressed this next.

#### 4.4 $MARS_{P_{2H}}$ RETAINS PERFORMANCE AMONGST RULE-BASED PREDICTIONS

We re-introduced inverse edges to  $MoA\text{-}net\text{-}10k$ , thereby restoring the ability to use reasoning shortcuts. Thereafter, we tested each of  $MARS_{P_{2H}}$ ,  $MARS_{\text{naive}}$ , and PoLo again (Fig. 2-E). While each approach was optimized for standard MRR, pruned metrics indicated how well positive predictions aligned with rules. In Fig. 2-E, we show that both MARS variants and PoLo achieved standard metrics on par with or better than  $MoA\text{-}net\text{-}10k$  without inverse edges (Fig. 2-D). However,  $MARS_{P_{2H}}$  also achieved pruned metrics comparable to its standard metrics, showing improved *calibration* rel-

ative to PoLo and  $\text{MARS}_{\text{naive}}$ . Finally, as in section 4.2, we used XSwap on *MoA-net-10k* to assess the susceptibility of  $\text{MARS}_{P_{2H}}$  to degree bias. Unlike in Section 4.2, we found no evidence for degree bias (see Appendix A.7).

#### 4.5 EXTERNAL VALIDATION OF $\text{MARS}_{P_{2H}}$ ON *MoA-net-10k*

In comparison to baseline methods,  $\text{MARS}_{P_{2H}}$ ’s metrics outperformed all but MINERVA’s, with which they were comparable (Table 1). However, since MINERVA does not, by design, utilize rules for guidance, it suffers the same reasoning shortcuts as PoLo and  $\text{MARS}_{\text{naive}}$ . In contrast to MINERVA, DWPC suffers the opposite limitation: predictions are based *only* on metapath-based rules.  $\text{MARS}_{P_{2H}}$ ’s *pruned* metrics, which are directly comparable, also outperform DWPC. Finally, as mentioned in Section 3.4, several drug-BP pairs corresponding to known MoAs in *Drug-MechDB* were included in the *MoA-net* test set. Of these, 33 pairs remained within *MoA-net-10k*’s test set, and  $\text{MARS}_{P_{2H}}$  recovered the correct MoA for all of them. Thus, this comprehensive benchmark highlights MARS’ ability to achieve near state-of-the-art performance by effectively balancing domain-specific knowledge with the capacity to generalize beyond it.

Table 1: Performance evaluations of MARS upon *MoA-net-10k* against baseline models. Metrics are presented as the (*average*, *standard deviation*) across five independent training/testing iterations. The best of each standard (top) and pruned (bottom) metric are in bold.

Model	metric type	Hits@1	Hits@3	Hits@10	MRR
ComplEx	standard	0.137	0.291	0.527	0.263
ConvE	standard	0.055	0.132	0.247	0.116
DistMult	standard	0.011	0.027	0.071	0.031
ER-MLP	standard	0.011	0.093	0.242	0.086
HoIE	standard	0.038	0.077	0.203	0.096
MURE	standard	0.071	0.181	0.253	0.177
RESCAL	standard	0.055	0.148	0.286	0.135
RotatE	standard	0.176	0.242	0.368	0.239
TransE	standard	0.154	0.297	0.538	0.274
MINERVA	standard	<b>(0.342, 0.016)</b>	<b>(0.516, 0.042)</b>	(0.66, 0.066)	<b>(0.45, 0.026)</b>
PoLo	standard	(0.272, 0.041)	(0.462, 0.054)	(0.606, 0.061)	(0.387, 0.044)
$\text{MARS}_{\text{naive}}$	standard	(0.33, 0.031)	(0.482, 0.066)	(0.664, 0.036)	(0.433, 0.036)
$\text{MARS}_{P_{2H}}$	standard	(0.23, 0.007)	(0.492, 0.027)	<b>(0.684, 0.03)</b>	(0.395, 0.016)
Metapaths with DWPC	pruned	0.370	0.560	0.780	0.508
PoLo	pruned	(0.17, 0.049)	(0.228, 0.061)	(0.228, 0.061)	(0.198, 0.052)
$\text{MARS}_{\text{naive}}$	pruned	(0.22, 0.049)	(0.238, 0.048)	(0.238, 0.048)	(0.229, 0.048)
$\text{MARS}_{P_{2H}}$	pruned	<b>(0.394, 0.026)</b>	<b>(0.644, 0.034)</b>	<b>(0.788, 0.018)</b>	<b>(0.535, 0.02)</b>

## 5 DISCUSSION

NeSy approaches are sometimes portrayed as more trustworthy than their black-box counterparts, partially due to increased interpretability (Gaur & Sheth, 2024; DeLong et al., 2024). Within this study, we enhanced the interpretability of a NeSy RL approach to produce our model,  $\text{MARS}_{P_{2H}}$ . Specifically, through our novel algorithm, two-hop joint probabilities ( $P_{2H}$ ), MARS learned weights corresponding to path-like rules, serving as a proxy for each rule’s importance. However, these insights revealed a new issue: NeSy RL approaches on KGs are susceptible to reasoning shortcuts. Specifically, in our study, predictions were driven by node degree bias. Ultimately, MARS’ enhanced interpretability called the trustworthiness of such approaches to question.

To address this, we considered Marconato et al. (2024a)’s desiderata for a shortcut-aware NeSy system. Specifically, on *MoA-net-10k*,  $\text{MARS}_{P_{2H}}$  showed both competitive *performance* as well as *calibration* in comparison to other models. Notably, however, measuring *calibration* is challenging in this domain. While rule-based predictions, measured through pruned metrics, follow the expected semantics for MoA deconvolution, we can not determine whether every *other* prediction follows *unintended* semantics. For example, in the classic MNIST addition task, popularly used to assess NeSy methods Manhaeve et al. (2018), a model is trained to determine the sum of two handwritten digits. In this toy example, the misclassification of a handwritten ‘2’ as ‘3’ and vice versa would still amount to the same sum. Thus, reasoning shortcuts can be objectively identified. On the contrary,

while we provide evidence that predictions using associative patterns are *largely* affected by node degree bias, we can not determine whether such patterns *always* reflect a reasoning shortcut.

Finally, regarding *cost effectiveness*,  $\text{MARS}_{P_{2H}}$  can be applied to any KG, serving as a generalizable mitigation strategy. However, we also note that this was achieved upon *MoA-net-10k*, a trimmed version of *MoA-net*. While we automated this trimming step, such a strategy does not make use of all available information. To scale  $\text{MARS}_{P_{2H}}$  to denser KGs and maintain its shortcut-aware status, several future directions could be explored. For instance, one could merge similar, high-degree nodes or rely upon domain knowledge, like the identification of promiscuous proteins (Copley, 2020), to make more informed choices about edge trimming or masking.

Our study highlights a key concern in which the behavior of some NeSy RL approaches could be attributed to node degree bias, rather than meaningful, domain-specific concepts. The interpretability of our approach,  $\text{MARS}_{P_{2H}}$ , allowed insight into this reasoning shortcut. Therefore, we question whether such shortcuts are identifiable amongst black-box approaches. Additionally, by testing a NeSy approach upon a novel applied task, MoA deconvolution, we could flag down patterns, like associative ones, which were plausible yet arguably less meaningful to biomedical researchers. Therefore, our study emphasizes the importance of testing interpretable models, like NeSy ones, in an applied domain. Finally, while our study honors the desiderata for shortcut-aware NeSy systems, we also examined the extent to which they were applicable to a biomedical domain.

## 6 CONCLUSIONS

We propose a novel prediction task for NeSy approaches on biomedical KGs: mechanism-of-action (MoA) deconvolution. In contrast to previous DD approaches, MoA deconvolution utilizes model interpretability to uncover the molecular mechanisms behind medicinal drugs. We also constructed a publicly available KG, *MoA-net*, for evaluating this task. To predict drug MoAs alongside indications, we designed the MoA Retrieval System (MARS). Relative to previous NeSy approaches, MARS has enhanced interpretability as it dynamically learns weights corresponding to logical rules. We showed that, with respect to the three desiderata for reasoning-aware NeSy systems, MARS has improved *calibration* and *cost effectiveness* compared to its predecessors, thereby enabling the identification and mitigation of a reasoning shortcut based on node degree bias.

### AUTHOR CONTRIBUTIONS

LND designed the methodology, wrote the software, and conducted the investigation. YG and LND did data curation and visualization. DDF and LND conceptualized the project. DDF, JDF, and PG supervised the project. All authors took part in writing the manuscript.

### ACKNOWLEDGMENTS

LND is funded by the University of Edinburgh Informatics Graduate School through the Global Informatics Scholarship. LND partially conducted this work during an internship at Enveda Bio-sciences Inc. JDF and PG are funded by the National Institute for Health Research (NIHR) Artificial Intelligence and Multimorbidity: Clustering in Individuals, Space and Clinical Context (AIM-CISC) grant NIHR202639. The views expressed are those of the author(s) and not necessarily those of the NIHR or the Department of Health and Social Care.

We thank these institutions for their support. We also thank Emile van Krieken and Guillermo Romero Moreno for their thoughtful feedback.

### REFERENCES

Kamal Acharya, Waleed Raza, Carlos Dourado, Alvaro Velasquez, and Houbing Herbert Song. Neurosymbolic reinforcement learning and planning: A survey. *IEEE Transactions on Artificial Intelligence*, 2023.

Mehdi Ali, Max Berrendorf, Charles Tapley Hoyt, Laurent Vermue, Sahand Sharifzadeh, Volker Tresp, and Jens Lehmann. Pykeen 1.0: a python library for training and evaluating knowledge graph embeddings. *The Journal of Machine Learning Research*, 22(1):3723–3728, 2021.

Ivana Balazevic, Carl Allen, and Timothy Hospedales. Multi-relational poincaré graph embeddings. *Advances in Neural Information Processing Systems*, 32, 2019.

Richard Bellman. A Markovian decision process. *Journal of mathematics and mechanics*, pp. 679–684, 1957.

Antoine Bordes, Nicolas Usunier, Alberto Garcia-Duran, Jason Weston, and Oksana Yakhnenko. Translating embeddings for modeling multi-relational data. *Advances in neural information processing systems*, 26, 2013.

A. Breit, S. Ott, A. Agibetov, and M. Samwald. Openbiolink: a benchmarking framework for large-scale biomedical link prediction. *Bioinformatics*, 39(13):4097–4098, 2020.

Zhe Chen, Yuehan Wang, Bin Zhao, Jing Cheng, Xin Zhao, and Zongtao Duan. Knowledge graph completion: A review. *IEEE Access*, 8:192435–192456, 2020. doi: 10.1109/ACCESS.2020.3030076.

Gene Ontology Consortium. The gene ontology resource: 20 years and still going strong. *Nucleic acids research*, 47(D1):D330–D338, 2019.

UniProt Consortium. Uniprot: a hub for protein information. *Nucleic acids research*, 43(D1):D204–D212, 2015.

Shelley D Copley. The physical basis and practical consequences of biological promiscuity. *Physical biology*, 17(5):051001, 2020.

Peter B Crino. The mtor signalling cascade: paving new roads to cure neurological disease. *Nature Reviews Neurology*, 12(7):379–392, 2016.

Rajarshi Das, Shehzaad Dhuliawala, Manzil Zaheer, Luke Vilnis, Ishan Durugkar, Akshay Krishnamurthy, Alex Smola, and Andrew McCallum. Go for a walk and arrive at the answer: Reasoning over paths in knowledge bases using reinforcement learning. In *ICLR*, 2018.

Sanjeeb Dash and Joao Goncalves. Lprules: Rule induction in knowledge graphs using linear programming. *arXiv preprint arXiv:2110.08245*, 2021.

Lauren Nicole DeLong, Ramon Fernández Mir, and Jacques D. Fleuriot. Neurosymbolic AI for reasoning over knowledge graphs: A survey. *IEEE Transactions on Neural Networks and Learning Systems*, pp. 1–21, 2024. doi: 10.1109/TNNLS.2024.3420218.

Tim Dettmers, Pasquale Minervini, Pontus Stenetorp, and Sebastian Riedel. Convolutional 2d knowledge graph embeddings. In *Proceedings of the AAAI conference on artificial intelligence*, volume 32, 2018.

Xin Dong, Evgeniy Gabrilovich, Jeremy Heitz, Wilko Horn, Ni Lao, Kevin Murphy, Thomas Strohmann, Shaohua Sun, and Wei Zhang. Knowledge vault: A web-scale approach to probabilistic knowledge fusion. In *Proceedings of the 20th ACM SIGKDD international conference on Knowledge discovery and data mining*, pp. 601–610, 2014.

Martin Drancé, Marina Boudin, Fleur Mougin, and Gayo Diallo. Neuro-symbolic xai for computational drug repurposing. In *KEOD*, pp. 220–225, 2021.

Adrià Fernández-Torras, Miquel Duran-Frigola, Martino Bertoni, Martina Locatelli, and Patrick Aloy. Integrating and formatting biomedical data as pre-calculated knowledge graph embeddings in the bioteque. *Nature Communications*, 13(1):5304, 2022.

Matthias Feurer and Frank Hutter. Hyperparameter optimization. *Automated machine learning: Methods, systems, challenges*, pp. 3–33, 2019.

H. Gan, X. Liu, Y. Liu, W. Chen, T. Dai, X. Xiao, and Y. Cao. Drugrep: an automatic virtual screening server for drug repurposing. *Acta Pharmacologica Sinica*, 44(4):888–896, 2023.

Anna Gaulton, Louisa J Bellis, A Patricia Bento, Jon Chambers, Mark Davies, Anne Hersey, Yvonne Light, Shaun McGlinchey, David Michalovich, Bissan Al-Lazikani, et al. Chemb3d: a large-scale bioactivity database for drug discovery. *Nucleic acids research*, 40(D1):D1100–D1107, 2012.

Manas Gaur and Amit Sheth. Building trustworthy neurosymbolic ai systems: Consistency, reliability, explainability, and safety. *AI Magazine*, 45(1):139–155, 2024.

Adriana Carolina Gonzalez-Cavazos, Anna Tanska, Michael Mayers, Denise Carvalho-Silva, Brindha Sridharan, Patrick A Rewers, Umasri Sankarlal, Lakshmanan Jagannathan, and Andrew I Su. Drugmechdb: A curated database of drug mechanisms. *Scientific Data*, 10(1):632, 2023.

A. Gottlieb, Y. Stein, E. Ruppin, and R Sharan. Predict: a method for inferring novel drug indications with application to personalized medicine. *Molecular systems biology*, 7(1):496, 2011.

R. Green, S. Mahalingaiah, M. Gopalakrishnan, J. Liguori, W. Mittelstadt, A. Blomme, and R. Van Vleet. Off-target pharmacological activity at various kinases: Potential functional and pathological side effects. *Journal of Pharmacological and Toxicological Methods*, 103, 2023.

Aric Hagberg, Pieter Swart, and Daniel S Chult. Exploring network structure, dynamics, and function using networkx. Technical report, Los Alamos National Lab.(LANL), Los Alamos, NM (United States), 2008.

Sami Hanhijärvi, Gemma C. Garriga, and Kai Puolamäki. Randomization techniques for graphs. In *Proceedings of the 2009 SIAM International Conference on Data Mining (SDM)*, pp. 780–791, 2009. doi: 10.1137/1.9781611972795.67.

Daniel Himmelstein, Benjamin Heil, Michael Zietz, Tong Shu Li, Kyle Kloster, Gregory Way, Casey Greene, and Sergio Baranzini. hetio/hetnetpy repository: Hetnets in Python, 2021. URL <https://github.com/hetio/hetnetpy>.

Daniel S Himmelstein and Sergio E Baranzini. Heterogeneous network edge prediction: a data integration approach to prioritize disease-associated genes. *PLoS computational biology*, 11(7):e1004259, 2015.

Daniel Scott Himmelstein, Antoine Lizée, Christine Hessler, Leo Brueggeman, Sabrina L Chen, Dexter Hadley, Ari Green, Pouya Khankhanian, and Sergio E Baranzini. Systematic integration of biomedical knowledge prioritizes drugs for repurposing. *Elife*, 6:e26726, 2017.

Sepp Hochreiter and Jürgen Schmidhuber. Long short-term memory. *Neural computation*, 9(8):1735–1780, 1997.

Yichen Jiang and Mohit Bansal. Avoiding reasoning shortcuts: Adversarial evaluation, training, and model development for multi-hop qa. *arXiv preprint arXiv:1906.07132*, 2019.

Mingxuan Ju, Tong Zhao, Wenhao Yu, Neil Shah, and Yanfang Ye. Graphpatcher: mitigating degree bias for graph neural networks via test-time augmentation. *Advances in Neural Information Processing Systems*, 36, 2024.

Bangzheng Li, Ben Zhou, Fei Wang, Xingyu Fu, Dan Roth, and Muhan Chen. Deceptive semantic shortcuts on reasoning chains: How far can models go without hallucination? In *Proceedings of the 2024 Conference of the North American Chapter of the Association for Computational Linguistics: Human Language Technologies (Volume 1: Long Papers)*, pp. 7668–7681, 2024a.

Mei Li, Xiangrui Cai, Sihan Xu, and Hua Ji. Metapath-aggregated heterogeneous graph neural network for drug–target interaction prediction. *Briefings in Bioinformatics*, 24(1):bbac578, 2023.

Zenan Li, Zehua Liu, Yuan Yao, Jingwei Xu, Taolue Chen, Xiaoxing Ma, and Jian Lü. Learning with logical constraints but without shortcut satisfaction. *arXiv preprint arXiv:2403.00329*, 2024b.

Xiaoqian Lin, Xiu Li, and Xubo Lin. A review on applications of computational methods in drug screening and design. *Molecules*, 25(6):1375, 2020.

Yushan Liu, Marcel Hildebrandt, Mitchell Joblin, Martin Ringsquandl, and Volker Tresp. Integrating logical rules into neural multi-hop reasoning for drug repurposing. *arXiv preprint arXiv:2007.05292*, 2020.

Robin Manhaeve, Sebastian Dumancic, Angelika Kimmig, Thomas Demeester, and Luc De Raedt. Deepprobabilog: Neural probabilistic logic programming. *Advances in neural information processing systems*, 31, 2018.

Emanuele Marconato, Samuele Bortolotti, Emile van Krieken, Antonio Vergari, Andrea Passerini, and Stefano Teso. Bears make neuro-symbolic models aware of their reasoning shortcuts. *arXiv preprint arXiv:2402.12240*, 2024a.

Emanuele Marconato, Stefano Teso, Antonio Vergari, and Andrea Passerini. Not all neuro-symbolic concepts are created equal: Analysis and mitigation of reasoning shortcuts. *Advances in Neural Information Processing Systems*, 36, 2024b.

Christoph Molnar. *Interpretable Machine Learning*. 2 edition, 2022. URL <https://christophm.github.io/interpretable-ml-book>.

Özlem Muslu, Charles Tapley Hoyt, Mauricio Lacerda, Martin Hofmann-Apitius, and Holger Fröhlich. Guiltytargets: prioritization of novel therapeutic targets with network representation learning. *IEEE/ACM Transactions on Computational Biology and Bioinformatics*, 19(1):491–500, 2020.

Maximilian Nickel, Volker Tresp, Hans-Peter Kriegel, et al. A three-way model for collective learning on multi-relational data. In *Icml*, volume 11, pp. 3104482–3104584, 2011.

Maximilian Nickel, Lorenzo Rosasco, and Tomaso Poggio. Holographic embeddings of knowledge graphs. In *Proceedings of the AAAI conference on artificial intelligence*, volume 30, 2016.

Ayush Noori, Michelle M Li, Amelia LM Tan, and Marinka Zitnik. Metapaths: similarity search in heterogeneous knowledge graphs via meta-paths. *Bioinformatics*, 39(5):btad297, 2023.

V. Palve, Y. Liao, R. Rix, , and U. Rix. Turning liabilities into opportunities: Off-target based drug repurposing in cancer. *In Seminars in cancer biology*, 68:209–229, 2021.

Florin Ratajczak, Mitchell Joblin, Martin Ringsquandl, and Marcel Hildebrandt. Task-driven knowledge graph filtering improves prioritizing drugs for repurposing. *BMC bioinformatics*, 23(1):84, 2022.

Alexandre Renaux, Chloé Terwagne, Michael Cochez, Ilaria Tiddi, Ann Nowé, and Tom Lenaerts. A knowledge graph approach to predict and interpret disease-causing gene interactions. *BMC bioinformatics*, 24(1):1–25, 2023.

Daniel J Rigden and Xosé M Fernández. The 2023 nucleic acids research database issue and the online molecular biology database collection. *Nucleic Acids Research*, 51(D1):D1–D8, 2023.

D. Rivas-Barragan, S. Mubeen, F. Guim Bernat, M. Hofmann-Apitius, and D. Domingo-Fernández. Drug2ways: Reasoning over causal paths in biological networks for drug discovery. *PLoS computational biology*, 16(12), 2020.

D. Rivas-Barragan, D. Domingo-Fernández, Y. Gadiya, and D. Healey. Ensembles of knowledge graph embedding models improve predictions for drug discovery. *Briefings in Bioinformatics*, 23 (6), 2022.

Stuart Russell and Peter Norvig. *Artificial intelligence: a modern approach*. Pearson, 2010.

B. Schultz, A. Zaliani, C. Ebeling, J. Reinshagen, D. Bojkova, and et al. Lage-Rupprecht, V. A method for the rational selection of drug repurposing candidates from multimodal knowledge harmonization. *Scientific reports*, 11(1):11049, 2021.

Prithviraj Sen, Breno WSR Carvalho, Ibrahim Abdelaziz, Pavan Kapanipathi, Francois Luus, Salim Roukos, and Alexander Gray. Combining rules and embeddings via neuro-symbolic ai for knowledge base completion. *arXiv preprint arXiv:2109.09566*, 2021.

Alex Sherstinsky. Fundamentals of recurrent neural network (rnn) and long short-term memory (lstm) network. *Physica D: Nonlinear Phenomena*, 404:132306, 2020.

Yizhou Sun, Rick Barber, Manish Gupta, Charu C Aggarwal, and Jiawei Han. Co-author relationship prediction in heterogeneous bibliographic networks. In *2011 International Conference on Advances in Social Networks Analysis and Mining*, pp. 121–128. IEEE, 2011.

Zhiqing Sun, Zhi-Hong Deng, Jian-Yun Nie, and Jian Tang. Rotate: Knowledge graph embedding by relational rotation in complex space. *arXiv preprint arXiv:1902.10197*, 2019.

Xianfeng Tang, Huaxiu Yao, Yiwei Sun, Yiqi Wang, Jiliang Tang, Charu Aggarwal, Prasenjit Mitra, and Suhang Wang. Investigating and mitigating degree-related biases in graph convolutional networks. In *Proceedings of the 29th ACM International Conference on Information & Knowledge Management*, pp. 1435–1444, 2020.

Théo Trouillon, Johannes Welbl, Sebastian Riedel, Éric Gaussier, and Guillaume Bouchard. Complex embeddings for simple link prediction. In *International conference on machine learning*, pp. 2071–2080. PMLR, 2016.

Fabio Urbina, Ana C. Puhl, and Sean Ekins. Recent advances in drug repurposing using machine learning. *Current Opinion in Chemical Biology*, 65(1):74–84, 2021.

Zonghan Wu, Shirui Pan, Fengwen Chen, Guodong Long, Chengqi Zhang, and S Yu Philip. A comprehensive survey on graph neural networks. *IEEE transactions on neural networks and learning systems*, 32(1):4–24, 2020.

Bishan Yang, Wen-tau Yih, Xiaodong He, Jianfeng Gao, and Li Deng. Embedding entities and relations for learning and inference in knowledge bases. *arXiv preprint arXiv:1412.6575*, 2014.

Y. Zheng, H. Peng, X. Zhang, Z. Zhao, X. Gao, and J. Li. Old drug repositioning and new drug discovery through similarity learning from drug-target joint feature spaces. *BMC bioinformatics*, 20:1–9, 2019.

Michael Zietz, Daniel S Himmelstein, Kyle Kloster, Christopher Williams, Michael W Nagle, and Casey S Greene. The probability of edge existence due to node degree: a baseline for network-based predictions. *GigaScience*, 13:giae001, 2024.

## A APPENDIX

### A.1 SELECTED METAPATHS

Table A1: Metapaths representing feasible MoAs. Drugs are represented with a  $D$ , proteins with a  $P$ , and biological processes with  $BP$ .

---

downregulates( $D, P$ ) $\rightarrow$ participates( $P, BP$ )
upregulates( $D, P$ ) $\rightarrow$ participates( $P, BP$ )
downregulates( $D, P$ ) $\rightarrow$ interacts( $P, P$ ) $\rightarrow$ participates( $P, BP$ )
upregulates( $D, P$ ) $\rightarrow$ interacts( $P, P$ ) $\rightarrow$ participates( $P, BP$ )
downregulates( $D, P$ ) $\rightarrow$ interacts( $P, P$ ) $\rightarrow$ interacts( $P, P$ ) $\rightarrow$ participates( $P, BP$ )
upregulates( $D, P$ ) $\rightarrow$ interacts( $P, P$ ) $\rightarrow$ interacts( $P, P$ ) $\rightarrow$ participates( $P, BP$ )

---

### A.2 IMPLEMENTATION

We implemented MARS using TensorFlow (version 2.10). The method is packaged in Python<sup>3</sup>. We used a grid search hyperparameter optimization (Feurer & Hutter, 2019); further details are within Appendix A.4.

The baseline KGE models have been trained using the PyKEEN framework (v1.10.1) (Ali et al., 2021). KGEMs were trained using PyKEEN’s hyperparameter optimization pipeline over 30 trials using as initial parameters the best configurations from (Rivas-Barragan et al., 2022). The evaluation in the hyperparameter optimization was conducted using Hits@10 for all the models on a link prediction task for the previously-described splits. Network algorithms were implemented in NetworkX (v3.1) (Hagberg et al., 2008) and metapaths were calculated using the hetnetpy Python package (Himmelstein et al., 2021; Himmelstein & Baranzini, 2015). Lastly, source code and data are openly available<sup>4</sup>.

### A.3 $P_{2H}$ FORMALIZATION

Here, we describe the weight updates in more detail. Both naive and  $P_{2H}$  updates are normalized according to expected values. For naive updates, we record observed frequency,  $O$ , at which each metapath-based rule is satisfied. This is normalized by the batch-specific expected frequency,  $E$ , in which every rule has a uniform probability across the total number rule groundings in that batch. For instance, if there are 10 metapath-based rules, and the agent satisfied at least one rule 100 times in a given batch,  $E$  would compute to 0.10, and each observed frequency  $O_M$ , would be normalized by  $E$ . If the agent found zero groundings, no weight updates would be made in that batch. Ultimately, this produces a metric,  $\mu$  (Eq. 3) in which any value over one indicates usefulness (the agent used that rule more than others), and any value less than one indicates otherwise.

$$\mu_{M_i} = O_{M_i} / E_{M_i} \quad (3)$$

Notably, the value of  $\mu$  was bound to avoid division by zero and extreme values. To adjust weight updates relative to the batch size and rollouts, we defined the minimum and maximum bounds on  $\mu$  as Eqs. 4 and 5, where  $\rho$  is the total number of metapath-based rules:

$$\mu_{min} = \frac{\rho}{\text{batch size} \times \text{rollouts}} \quad (4)$$

$$\mu_{max} = \rho \times \text{batch size} \times \text{rollouts} \quad (5)$$

<sup>3</sup><https://github.com/laurendelong21/MARS>

<sup>4</sup><https://github.com/laurendelong21/MoA-Net>

Using Eq. 6, denoted by  $\Phi$ ,  $\mu$  (Eq. 3) is used to update the weight of a rule,  $w(M_i)$ . Eq. 6 is regularized by the hyperparameter  $\alpha \in \mathbb{R}$ , where  $0 \leq \alpha \leq 1$  to control how drastic the weight update is. An  $\alpha$  closer to zero indicates subtle updates; this might be suitable if the user wants weights to act as a gauge on relative importance between rules. An  $\alpha$  closer to one indicates drastic updates and could be suitable if the user has many rules and wants those which are less useful to be reduced to zero. If  $\alpha = 0$ , no weight updates will be made. Therefore,  $\alpha$  can be selected based on user needs or via hyperparameter optimization.

$$\Phi(\mu, w(M_i)) = w(M_i) \times 2\alpha \left( \frac{\mu - 1}{\mu + 1} \right) \quad (6)$$

The second, more complex method by which weight updates were done is based on a term we coined, *two-hop joint probability*,  $P_{2H}$ . Pseudocode for  $P_{2H}$  can be found in Algorithm 1 below. This metric approximates the usefulness of metapath-based rules based on the observed frequencies of the two-hop fragments which they comprise. Here, the main differences are that (1) Eq. 3 is computed based on the observed and expected probabilities of two-hop fragments, rather than whole metapaths, and (2)  $\rho$  within Equations 4 and 5 is the number of unique two-hop fragments possible.

---

**Algorithm 1**  $P_{2H}$  weight updates

---

```

for each batch,  $\beta$  do
     $\mathcal{F} \leftarrow$  [empty list]
    for each path,  $\mathcal{P}$ , that the agent traverses, do
        if the agent found a true pair then
             $\hat{P} \leftarrow \text{metapath}(\mathcal{P})$                                  $\triangleright$  extract the metapath
             $\mathcal{F} \leftarrow \mathcal{F} + \text{extract\_fragments}(\hat{P})$            $\triangleright$  a list of two-hop fragments seen
        end if
    end for
     $E \leftarrow 1 / \text{num. unique fragments in } \mathcal{F}$ 
    for each unique fragment,  $f$ , in  $\mathcal{F}$  do
         $O_f \leftarrow \text{count}(f)$ 
    end for
    for each metapath-based rule body,  $M_i$ , in  $\mathcal{M}$  do
         $\theta \leftarrow \text{extract\_fragments}(M_i)$                                  $\triangleright$  a list of the fragments in the metapath
         $P_{2H}(M_i) \leftarrow \prod_{f=1}^{\text{len}(\theta)} \frac{O_f}{E}$            $\triangleright$  ratio of observed / expected frequency, as in Eq. 3
         $w(M_i) \leftarrow \Phi(P_{2H}(M_i), w(M_i))$            $\triangleright$  use Eq. 6 to adjust rule weight
    end for
end for

```

---

#### A.4 HYPERPARAMETER SELECTION

Here, we describe hyperparameter selection. Table A2 describes the hyperparameter search space for optimization, and Table A3 describes the hyperparameters which were fixed for every model.

Table A2: Hyperparameter search space for grid search optimization (Feurer & Hutter, 2019)

Hyperparameter	Description	Search space
$\lambda$ (Lambda)	ratio at which the second summand is applied relative to the first summand in the reward function	{5, 8, 10}
$\alpha$ (alpha)	how dramatically weight updates should be made (if applicable)	{0.001, 0.01, 0.1}
learning rate	learning rate of the optimizer	{0.0001, 0.001, 0.01}
hidden size	size of hidden layers	{64 128 256}
batch size	size of sampled mini-batch for training	{128, 256}
rollouts	number of times each query (source-terminal node pair) is made or attempted during training	{50, 100}
$\gamma_{\text{baseline}}$ (gamma baseline)	discount factor for the baseline	{0.05, 0.5}
$\beta$ (beta)	entropy regularization factor	{0.025 0.05}

Table A3: Fixed hyperparameter settings

Hyperparameter	Description	Value
embedding size	size of the relation and entity embeddings	256
LSTM layers	number of LSTM layers	2
test rollouts	number of times each query (source-terminal node pair) is made or attempted during testing	50
max branching	maximum number of outgoing edges per node shown to the agent in an episode	150
$\gamma$ (gamma)	discount factor	1
positive reward	reward for finding a true pair	1
negative reward	penalty for failing to find a true pair	0

#### A.5 POLO METRICS WITHOUT ASSOCIATIVE RULES

We ran PoLo on the *Hetionet* KG (Himmelstein et al., 2017) using the same parameters and data splits as reported by Liu et al. (2020). In contrast to Liu et al. (2020), we input all directed metapaths of length  $L \leq 4$  as rule bodies (as in Appendix A.1). These metapaths served as the metapath-based rules for PoLo. Notably, these metapaths excluded the associative metapath mentioned in section 4.1:

$$\text{treats}(\text{Drug}_1, \text{Disease}) \Leftarrow \text{causes}(\text{Drug}_1, \text{Side Effect}) \wedge \text{causes}(\text{Drug}_2, \text{Side Effect}) \wedge \text{treats}(\text{Drug}_2, \text{Disease})$$

Despite the most-used metapath-based rule being absent, PoLo achieved the same standard metrics as previously reported (Table A4).

Table A4: Performance evaluations of PoLo upon *Hetionet* as reported in Liu et al. (2020) (*average* across five independent training/testing iterations) and PoLo upon *Hetionet* *without* associative rules (*average, standard deviation*) across four independent training/testing iterations.)

rule types	Hits@1	Hits@3	Hits@10	MRR
associative ((Liu et al., 2020))	0.314	0.428	0.609	0.402
mechanistic (this study)	(0.328, 0.046)	(0.465, 0.037)	(0.656, 0.044)	(0.431, 0.035)

## A.6 ABLATION STUDY

Here, we tested the effects of reducing the test set size ( $n=100$ ) on performance. The lack of change between Fig. 4-C and C (test=100) indicates that a reduction in test set size is not responsible for improvements observed in Fig. 4-D.

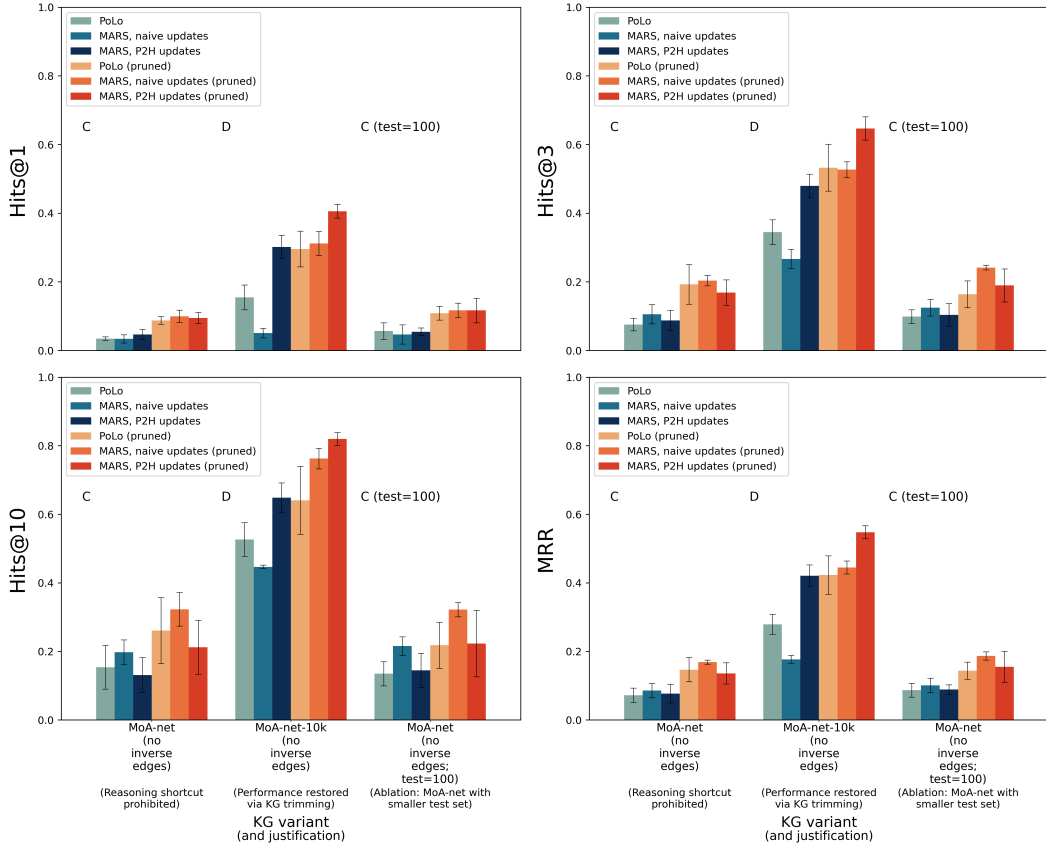


Figure 4: Performance evaluations upon *MoA-net* (no inverse edges) with a test set of 100 triples. Metrics are presented as the average, with error bars representing standard deviation across five independent training/testing iterations. The lack of change between C and C (test=100) indicates that a reduction in test set size is not responsible for improvements observed in D.

### A.7 XSWAP PERMUTATIONS: $\text{MARS}_{P_{2H}}$ ON *MoA-net-10k*

Using the XSwap algorithm as in Section 4.2, we checked, once again, whether the prediction metrics achieved using  $\text{MARS}_{P_{2H}}$  on *MoA-net-10k* were influenced by degree bias. This time, there was a stark decrease in performance metrics upon the permuted KG (Fig. 5). This showed that predictions made by  $\text{MARS}_{P_{2H}}$  were due to factors beyond node degree bias.

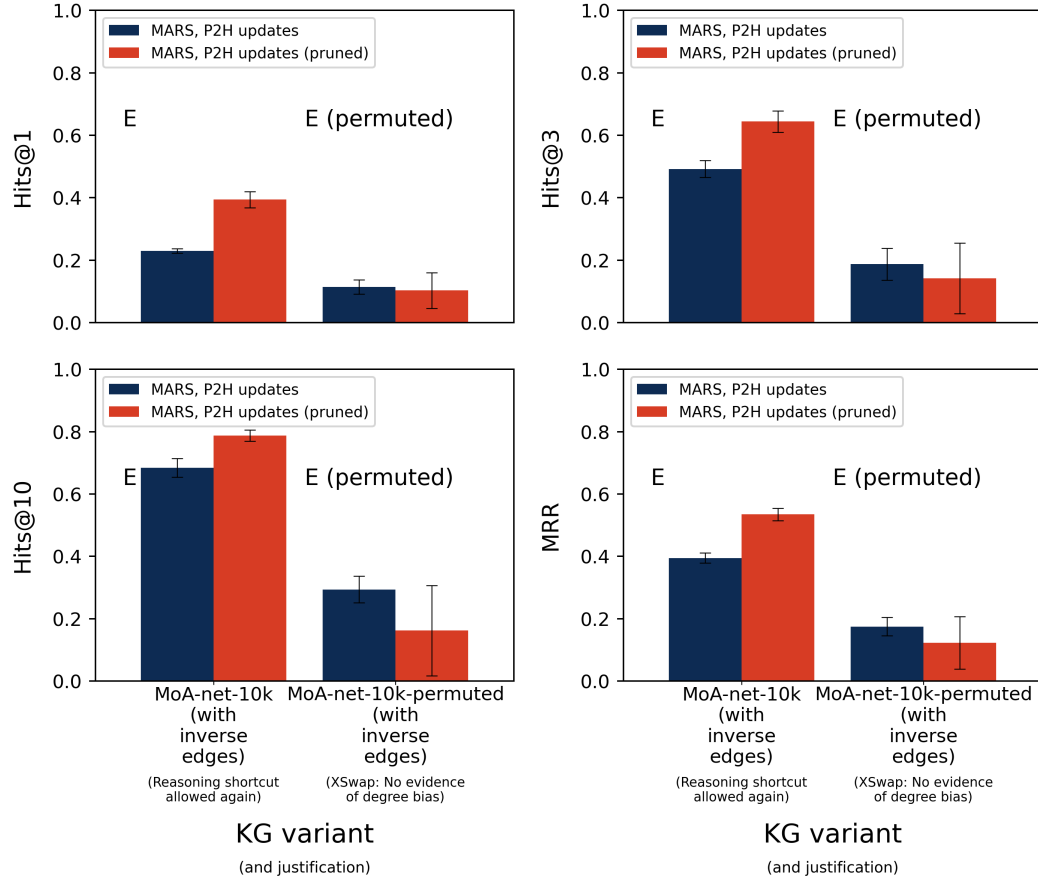


Figure 5: Performance evaluations of  $\text{MARS}_{P_{2H}}$  on *MoA-net-10k* as well as a permuted variant of *MoA-net-10k* via the XSwap algorithm. Metrics are presented as the average, with error bars representing standard deviation across five independent training/testing iterations. A drop in performance metrics (E (permuted)) indicates that node degree was not the main driver in predictions made in E.